Multi-harmonic modulation in a fiber-optic gyroscope

Martin Miranda,[1,*] Nobuyuki Takei,[1,2] Yuki Miyazawa,[1] and Mikio Kozuma[1,3,†]

[1] *Institute of Innovative Research, Tokyo Institute of Technology, 4259 Nagatsuta-cho, Midori-ku, Yokohama, Kanagawa 226-8503 Japan*
[2] *MIZUSAQI Inc., 1-48-3 Hanasaki-cho, Naka-ku, Yokohama, Kanagawa 231-0063 Japan.*
[3] *Department of Physics, Tokyo Institute of Technology, 2-12-1 O-Okayama, Meguro-ku, Tokyo 152-8550 Japan.*

Optimizing the bias modulation of a fiber-optic gyroscope is crucial to improving its precision. In this study, we propose and demonstrate the use of multiple harmonics of sinusoidal modulation as an intermediate alternative to the widely used modulation methods: sinusoidal and square-wave modulation. We show that this alternative integrates the advantages of each modulation method by providing a smooth modulation that produces a clean, spike-free output and a satisfactory signal-to-noise ratio. By using three harmonics of modulation in combination with a high frequency to reduce thermal phase noise, we obtained an angular random walk of $5.2(2)\mu\text{deg}/\sqrt{\text{h}}$ and a bias instability of $\sim 10\mu$deg/h.

I. INTRODUCTION

Inertial rotational motion detection is an essential requirement in the fields of inertial navigation and geophysics. Based on the Sagnac effect, interferometric fiber-optic gyroscopes (FOGs) measure the phase difference of two counterpropagating light waves traveling through a fiber coil. In recent years, FOGs have received extensive attention and research [1] because of their light weight, high reliability, wide dynamic range, and long life.

For demanding applications, including inertial navigation and geophysics, improving the precision of an FOG is crucial. The precision of an FOG can be improved by either increasing its scale factor, which is proportional to the coil diameter and length, or reducing its amount of phase noise [2]. Giant FOGs with large coil diameters of over a meter are promising for studying geophysical phenomena [2, 3]. Using longer fibers is also possible at the expense of increased shot noise contributions due to optical attenuation. While considering the effects of shot noise, the optimal coil length is a few kilometers [4].

Reducing phase noise is especially important in applications regarding inertial navigation because the precision can be improved without increasing the size of the coil [2]. In an FOG interrogated by incoherent light, four types of noise dominate [5]: relative-intensity noise (RIN) [6–9], thermal-phase noise (TPN) [10–12], shot noise (SN), and detection noise (DN). While SN and DN can be kept sufficiently small using high-power laser sources and low-noise detection instruments, ultimately, RIN and TPN are the limiting factors in current FOGs. To reduce TPN, high modulation frequencies can be used. This has been demonstrated in previous experiments that are based on using a 30 km-long single-mode (SM) fiber coil [13]. Several techniques were demonstrated to reduce the effects of RIN: using noise subtraction by either electronic [14] or optical [15–17] means; with an interferometric filter [18]; with a fiber ring resonator [19]; using a semiconductor amplifier [20]; and by current feedback [21].

To properly identify the rotation direction, an FOG utilizes dynamic biasing phase modulation. Optimization of the bias modulation is essential for reducing the phase noise [22]. Two different types of modulation are used on FOGs: sinusoidal and square-wave modulation (SWM). Sinusoidal modulation is popular in open-loop-based FOG since it can be easily achieved with commercial lock-in amplifiers. On the other hand, in terms of maximizing the ratio between the sensitivity and RIN, SWM is preferred [22]. This is because the signal is proportional to $\sin(\phi)$, where ϕ is the modulation amplitude, while RIN is proportional to $1 + \cos(\phi)$. Regarding a modulation depth near $\phi = \pi$, both the signal and RIN converge to zero, but the signal-to-noise ratio diverges to infinity [22].

Unfortunately, using SWM has disadvantages. When the modulation voltage switches at a finite speed, spikes are generated in the detected signal. Spikes can be partially removed from the signal by analog or optical switching [22] or digital processing. However, since the temporal shape of the spike is determined only by the bandwidth of the modulation and detection elements and is independent of the frequency, the temporal density of spikes increases with frequency. A large portion of the signal must be removed at high modulation frequencies, which deteriorates the sensitivity. Therefore, the following dilemma arises: choosing a high modulation frequency that favors TPN reduction or using SWM, which reduces RIN but is incompatible with high modulation frequencies due to the spike problem.

In this paper, we propose the use of multi-harmonic modulation for solving this dilemma. A modulation signal with multiple harmonics is given by:

$$\phi_{\text{mod}} = \sum_{n=1}^{N_{\text{h}}} \phi_{2n-1} \sin(2n-1)\omega t \tag{1}$$

* miranda@qnav.iir.titech.ac.jp
† kozuma@qnav.iir.titech.ac.jp

where ω and ϕ_{2n-1} are the odd-order harmonic of the fiber-coil eigenfrequency and the modulation depth, respectively. This includes the sinusoidal wave modulation case for $N_\mathrm{h} = 1$ and the square-wave modulation for $N_\mathrm{h} \to \infty$, given by:

$$\phi_\mathrm{sq} = \frac{4\phi}{\pi} \sum_{n=1}^{\infty} \frac{1}{2n-1} \sin(2n-1)\omega t. \tag{2}$$

where ϕ is the amplitude of the square wave. We show that choosing a multi-harmonic bias modulation that is sufficiently close to a square wave modulation can reduce the RIN effects. Additionally, since this modulation does not generate spikes, it can be applied at high frequencies to reduce TPN. The goals of this work are to derive theoretical formulas for multi-harmonic modulation, obtain optimal parameters for modulation, and experimentally verify its potential . In particular, we focus on the cases for $N_\mathrm{h} = 1$, 2 and 3 corresponding to single-harmonic modulation (SHM), dual-harmonic modulation (DHM) and triple-harmonic modulation (THM), respectively.

II. THEORY OF MULTI-HARMONIC MODULATION

First, SHM will be reviewed. The output of the photodetector is given by:

$$S = \frac{I_0}{2} \Re \left(1 + e^{i\theta} e^{i\phi_1 \sin \omega t}\right), \tag{3}$$

where I_0 is the current at the photodetector without rotation and modulation and θ is the Sagnac phase. The Jacobi-Anger expansion can be used to obtain:

$$e^{i\phi_1 \sin \omega t} = \sum_{n=-\infty}^{\infty} J_n(\phi_1) e^{in\omega t} \tag{4}$$

where $J_n(\phi_1)$ is the n-th order ordinary Bessel function (OBF) of the first kind. Moreover, we obtain:

$$S = \frac{I_0}{2} \Re \left(1 + e^{i\theta} \sum_{n=-\infty}^{\infty} J_n(\phi_1) e^{in\omega t}\right). \tag{5}$$

The demodulated, fundamental harmonic of the signal results in:

$$S_{1\omega} = \int_{-\infty}^{\infty} S \sin(\omega t) dt = -I_0 \sin\theta J_1(\phi_1). \tag{6}$$

Similarly, the output of the photodetector modulated by DHM is:

$$S = \frac{I_0}{2} \Re \left(1 + e^{i\theta} e^{i\phi_1 \sin \omega t + i\phi_3 \sin 3\omega t}\right). \tag{7}$$

We can now introduce the two-dimensional generalized Bessel function (GBF) [23, 24], with a Jacobi-Anger expansion given by:

$$e^{i(u \sin p\omega t + v \sin q\omega t)} = \sum_{n=-\infty}^{\infty} J_n^{p,q}(u,v) e^{in\omega t} \tag{8}$$

Then, the photodetector signal results in:

$$S = \frac{I_0}{2} \Re \left(1 + e^{i\theta} \sum_{n=-\infty}^{\infty} J_n^{1,3}(\phi_1, \phi_3) e^{in\omega t}\right). \tag{9}$$

Since this equation is in the same form as Eq. (5) except for a different factor multiplying $e^{in\omega t}$, it follows that:

$$S_{1\omega} = -I_0 \sin\theta J_1^{1,3}(\phi_1, \phi_3). \tag{10}$$

The two-dimensional GBF can be decomposed into ordinary Bessel functions:

$$J_n^{p,q}(u,v) = \sum_{k,l \in \mathbb{Z}, pk+ql=n} J_k(u) J_l(v) \tag{11}$$

For $\phi_3 = 0$, the following can be obtained:

$$J_n^{1,3}(\phi_1, 0) = \sum_{k,l \in \mathbb{Z}, k+3l=n} J_k(\phi_1) J_l(0) = J_n(\phi_1), \tag{12}$$

and Eq. (10) reverts to Eq. (6), that is, the SHM case.

As seen with Eqs. (5) and (9), any Jacobi-Anger expansion in the SHM case can be expressed in an equivalent form for the DHM case by just replacing the OBF with the GBF. Using this property, known equations for RIN and SN [21] can be easily extended to the DHM case to obtain:

$$\sigma_\mathrm{RIN} = \frac{\eta I_0 \sqrt{B}}{2\sqrt{\Delta\nu}} \Bigg\{ \left[1 + J_0^{1,3}(\phi_1, \phi_3) - J_2^{1,3}(\phi_1, \phi_3)\right]^2 + \sum_{n=1}^{\infty} \left[J_{2n}^{1,3}(\phi_1, \phi_3) - J_{2n+2}^{1,3}(\phi_1, \phi_3)\right]^2 \Bigg\}^{1/2} \tag{13a}$$

$$\sigma_\mathrm{SN} = \left\{ \frac{eI_0 B}{2} \left[1 + J_0^{1,3}(\phi_1, \phi_3) - J_2^{1,3}(\phi_1, \phi_3)\right] \right\}^{1/2} \tag{13b}$$

where B, $\Delta\nu$, η and e are the detection bandwidth, laser spectrum bandwidth, attenuation factor related to semiconductor gain effects, and electron charge, respectively.

Additionally, this analysis can be further extended to the THM case using the three-dimensional GBF [24] given by:

$$e^{i(u \sin p\omega t + v \sin q\omega t + w \sin r\omega t)} = \sum_{n=-\infty}^{\infty} J_n^{p,q,r}(u,v,w) e^{in\omega t} \tag{14a}$$

$$J_n^{p,q,r}(u,v,w) = \sum_{k,l,m \in \mathbb{Z}, pk+ql+rm=n} J_k(u) J_l(v) J_m(w). \tag{14b}$$

The equations for an increased number of harmonics $N_\mathrm{h} > 3$ are straightforward.

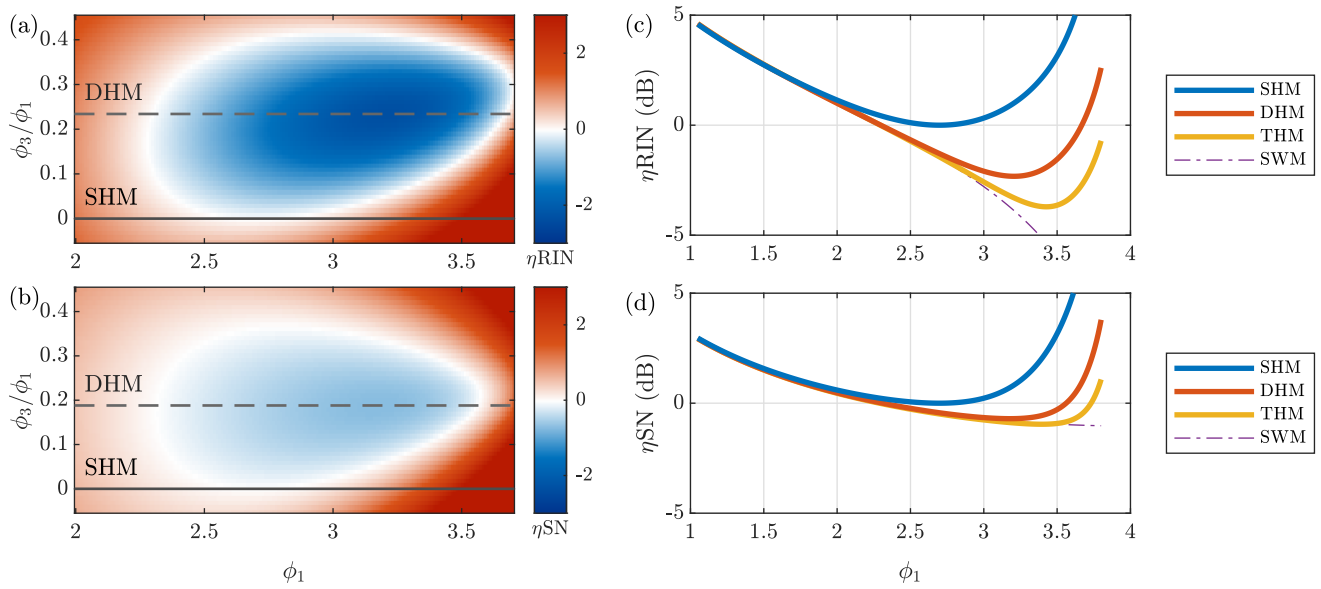

FIG. 1. Improvement of RIN- and SN-induced ARW for multi-harmonic modulation. Improvement units are in dB. (a)(b): η_{RIN} and η_{SN} as a function of ϕ_1 and ratio ϕ_3/ϕ_1. SHM and optimal DHM ratios ϕ_3/ϕ_1 are shown as solid and dashed lines, respectively. (c) η_{RIN} as a function of ϕ_1 for fixed ratios: $\phi_3/\phi_1 = 0.234$ for DHM; $\phi_3/\phi_1 = 0.288$ and $\phi_5/\phi_1 = 0.118$ for THM. (d) η_{SN} as a function of ϕ_1 for fixed ratios: $\phi_3/\phi_1 = 0.188$ for DHM; $\phi_3/\phi_1 = 0.235$ and $\phi_5/\phi_1 = 0.080$ for THM. For comparison, the SWM case is shown as a function of $4\phi/\pi$ in (c) and (d).

III. MODULATION INDEX OPTIMIZATION

The theoretical formulas for the signal and each of the noises can be used to obtain the optimal set of modulation depths (ϕ_1, ϕ_3, ϕ_5) that minimize RIN- or SN-induced ARW; this set is defined by:

$$\mathrm{ARW}_{\mathrm{RIN}}(\phi_1,\phi_3,\phi_5) = \frac{\sigma_{\mathrm{RIN}}}{S_F I_0 J_1^{1,3,5}(\phi_1,\phi_3,\phi_5)\sqrt{B}} \quad (15a)$$

$$\mathrm{ARW}_{\mathrm{SN}}(\phi_1,\phi_3,\phi_5) = \frac{\sigma_{\mathrm{SN}}}{S_F I_0 J_1^{1,3,5}(\phi_1,\phi_3,\phi_5)\sqrt{B}} \quad (15b)$$

respectively [21]. Here, $S_F = 4\pi RL/c\lambda$ is the scale factor of a fiber coil with a radius of R and a length of L. Moreover, c and λ correspond to the speed of light and central wavelength of the light source, respectively. To perform the analysis, it is convenient to plot ARW values as a function of the modulation index ϕ_1 and the ratios $(\phi_3/\phi_1, \phi_5/\phi_1)$, which determine the depth and temporal shape of the modulation signal, respectively.

Theoretical calculations on ARW to obtain the DHM are shown in Figs. 1(a) and 1(b). To compare the performance of the DHM and THM with that of the SHM, we introduced improvement factors:

$$\eta_{\mathrm{RIN}} = \frac{\mathrm{ARW}_{\mathrm{RIN}}(\phi_1,\phi_3,\phi_5)}{\mathrm{ARW}_{\mathrm{RIN}}(2.70,0,0)} \quad (16a)$$

$$\eta_{\mathrm{SN}} = \frac{\mathrm{ARW}_{\mathrm{SN}}(\phi_1,\phi_3,\phi_5)}{\mathrm{ARW}_{\mathrm{SN}}(2.70,0,0)}, \quad (16b)$$

which normalize the ARW to the optimal case for the SHM occurring at $\phi_1 = 2.70$. For $\mathrm{ARW}_{\mathrm{RIN}}$ in the DHM, the optimal modulation is $(\phi_1, \phi_3) = (3.21, 0.75)$, which results in a 2.3dB improvement in the ARW. SN-induced ARW also improves by 0.7dB at $(\phi_1, \phi_3) = (3.18, 0.60)$. For reference, we included results for negative ratios $-0.05 < \phi_3/\phi_1 < 0$ in Figs. 1(a) and (b), which correspond to the case of a sinusoidal wave approximating a triangular wave. In general, negative ratios of ϕ_3/ϕ_1 deteriorate both $\mathrm{ARW}_{\mathrm{RIN}}$ and $\mathrm{ARW}_{\mathrm{SN}}$.

Figs. 1(c) and (d) show the improvement factor dependence on the modulation index ϕ_1 for the SHM, DHM, THM, and SWM. Here, we fixed the modulation index ratios for the DHM and THM to the value that minimize the ARW for each noise. One can see that incorporating more harmonics improves the ARW, and the improvement factor converges to that of the SWM. Optimal values of the SHM, DHM, and THM are summarized in Table I.

According to the Fourier decomposition of a square wave in Eq. (2), the modulation index ratios ϕ_3/ϕ_1 and ϕ_5/ϕ_1 that best approximate a modulation wave to a square wave are $(\phi_3, \phi_5)/\phi_1 = (1/3, 1/5)$. Contrary to

TABLE I. Optimal modulation indexes for SHM, TWM and THM that minimize $\mathrm{ARW}_{\mathrm{RIN}}$ and $\mathrm{ARW}_{\mathrm{SN}}$. Improvement factors are shown in dB units.

	RIN				Shot Noise			
	ϕ_1	ϕ_3	ϕ_5	η_{RIN}	ϕ_1	ϕ_3	ϕ_5	η_{SN}
SHM	2.70	0	0	0	2.70	0	0	0
DHM	3.21	0.75	0	−2.3	3.18	0.60	0	−0.7
THM	3.42	0.99	0.41	−3.7	3.40	0.80	0.27	−1.0

expectations, these ratios are not optimal for minimizing the ARW. It can be demonstrated through numerical calculations that optimal ratios will eventually converge to $\phi_{2n-1}/\phi_1 = \frac{1}{2n-1}$ for $N_\mathrm{h} \to \infty$, which corresponds to the SWM.

IV. EXPERIMENTAL SETUP

The experimental setup is shown in Fig. 2. The optical source is composed of a super-luminescent diode (SLD) with a central wavelength of 1544 nm, bandwidth of 52 nm, and output power of 40 mW amplified by a semiconductor optical amplifier (SOA). The SOA has two important roles: it amplifies the output of the SLD to 100 mW and reduces the RIN due to the gain saturation effect [20]. By comparing the noise measured directly after the SLD and SOA, we estimate a 11.2 dB improvement in RIN. The output of the SOA goes through an optical circulator (OC) to a multifunctional integrated optical chip (MIOC). The output of the MIOC is spliced to a quadrupolar-wound coil having a length of $L = 4920$ m and an average radius of $R = 115$ mm. The return path of the optical circulator is inputted to a photodetector (PD), resulting in an output of $I_0 = 4$ mA. We positioned the fiber coil and MIOC inside a temperature-stabilized vacuum chamber to reduce long-time drift effects.

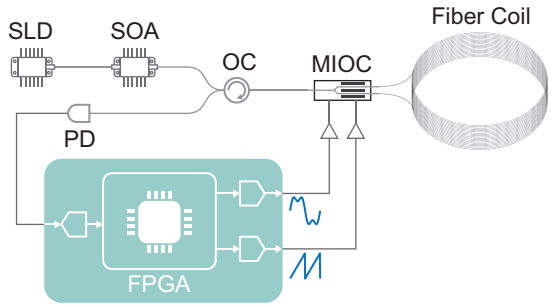

FIG. 2. Schematic setup of the experimental apparatus. SLD, super-luminescent diode; SOA, semiconductor optical amplifier; OC, optical circulator; MIOC, multifunctional integrated optical chip; PD, photodetector.

The Sagnac phase detection system is a digital-closed-loop detection scheme built around a field-programmable gate array (FPGA) based on a Zynq 7020 SoC. Bias and serrodyne modulation signals are generated by a digital-analog converter (AD9747) followed by a homemade amplifier. Digital generating the bias signal is crucially important for multi-harmonic modulation, as it ensures that the relative amplitude and phase between different harmonics remain constant. The output of the PD is read by an analog-digital converter (LTC2157-14) and demodulated digitally using sinusoidal demodulation.

We employ the 101st harmonic of the coil eigenfrequency for modulation, which is given by $\omega/2\pi = 101 f_c = 2.05$ MHz. At this frequency, the TPN is comparable to SN and DN. This will be analyzed in detail in the next section.

V. EXPERIMENTAL RESULTS

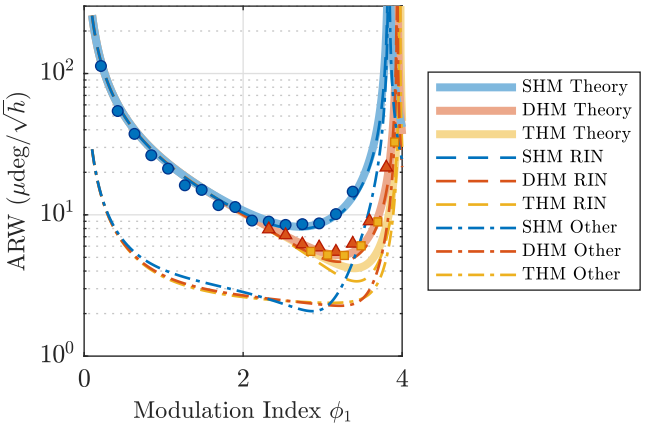

FIG. 3. ARW dependence on the modulation frequency ϕ_1 for SHM, DHM ($\phi_3/\phi_1 = 0.234$) and THM ($(\phi_3, \phi_5)/\phi_1 = (0.288, 0.118)$) denoted by circular, triangular and square points, respectively. Solid lines: Total estimated ARW including all sources of noise. Dashed lines: RIN-induced ARW. Dashed-dotted lines: SN-, DN- and TPN-induced ARW.

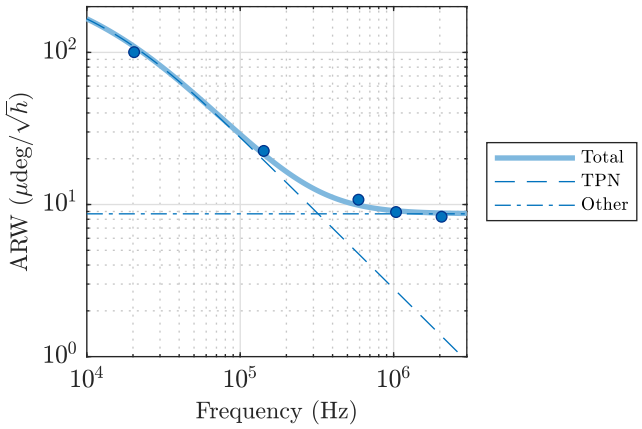

FIG. 4. Modulation frequency dependency of the ARW for the SHM case. Solid dots: Experimental results. Solid line: ARW including all sources of noise. Dashed line: TPN contribution to ARW. Dashed-dotted lines: Sum of other noise-induced ARW, including SN, DN and RIN.

We experimentally verify the improvement in the ARW by measuring its dependency on ϕ_1 for the fixed ratios $(\phi_3, \phi_5)/\phi_1 = (0.234, 0)$ for DHM and $(\phi_3, \phi_5)/\phi_1 = (0.288, 0.118)$ for THM, corresponding to the optimal ratios that minimize the RIN effects. The results are shown in Fig. 3. Each value was estimated by fitting the Allan deviation during one hour of measurement. The best

ARW values obtained for SHM, DHM and THM were $8.5(2)\mu\text{deg}/\sqrt{\text{h}}$, $5.5(4)\mu\text{deg}/\sqrt{\text{h}}$ and $5.2(2)\mu\text{deg}/\sqrt{\text{h}}$, respectively, which translates to a 1.9 dB improvement for DHM and 2.2 dB for THM. Solid lines indicate the theoretical estimation for ARW including all sources of noise (RIN, TPN, SN and DN).

We estimated the RIN (dashed lines in Fig. 3) by switching off the modulation and measuring the noise in the detector in open-loop mode. Since RIN is one order of magnitude larger than SN, the resultant noise is dominated by RIN. The estimated attenuation factor was $\eta = 0.15$. Detection noise was estimated in the same manner with the input light in the PD removed. The measured DN was 3% of RIN in the absence of modulation. Other noise-induced ARWs, shown in dashed-dotted lines in Fig. 3, include the effects of SN, DN and TPN.

To estimate the amount of TPN, we measured the dependency of the ARW on the modulation frequency for the SHM case. TPN-induced ARW is given by:

$$\text{ARW}_{\text{TPN}} = \frac{\sigma_{\text{TPN}}}{S_F I_0 J_1(\phi_1)\sqrt{B}} \tag{17a}$$

$$\sigma_{\text{TPN}} = I_0 \left\{ \pi B \sum_{n=1}^{\infty} \left[J_{2n-1}(\phi_1) - J_{2n+1}(\phi_1) \right]^2 \times \langle \Delta\phi^2_{N,\text{rms}}(2n\omega) \rangle \right\}^{1/2} \tag{17b}$$

where

$$\langle \Delta\phi^2_{N,\text{rms}}(2n\omega) \rangle = \frac{k_B T^2 L}{\kappa \lambda^2} \left(\frac{dn_{\text{eff}}}{dT} + n_{\text{eff}} \alpha_L \right)^2 \times \ln \left[\frac{\left(\frac{2}{W_0}\right)^4 + \left(\frac{2n\omega}{D}\right)^2}{\left(\frac{4.81}{d}\right)^2 + \left(\frac{2n\omega}{D}\right)^2} \right] \left[1 - \text{sinc}\left(\frac{2n\omega L n_{\text{eff}}}{c} \right) \right] \tag{18}$$

is the spectral density of phase noise introduced by the TPN. k_B, T, κ, n_{eff}, α_L, W_0 and D are the Boltzmann's constant, the temperature of the coil, thermal conductivity, effective refractive index of the fiber, linear thermal expansion coefficient, mode field radius and thermal diffusivity, respectively. Typical values can be found in different studies [11, 13, 21].

The experimental results are shown in Fig. 4. Since the other sources of noise can be considered independent of the modulation frequency, the data can be fitted by:

$$\text{ARW} = \sqrt{\text{ARW}^2_{\text{TPN}}(\omega; D) + \text{ARW}^2_{\text{other}}} \tag{19}$$

where the fitting parameters are the thermal diffusivity of the optical fiber D and a constant $\text{ARW}_{\text{other}}$ that includes RIN, DN and SN contributions to the ARW. This resulted in $D = 1.0(1) \times 10^{-6}\text{m}^2\text{s}^{-1}$ and $\text{ARW}_{\text{other}} = 8.7(8)\mu\text{deg}/\sqrt{\text{h}}$. We found no discrepancy between the obtained thermal diffusivity value and the value for bulk fused silica found in the literature [11, 13, 25].

The estimated contributions of RIN, DN, SN and TPN to ARW are summarized in Table II. For a modulation frequency of 2.05 MHz, the TPN contribution to the ARW is comparable to the sum of the DN and SN contributions. Consequently, a further increase in the modulation frequency will result in a negligible improvement in the ARW. On the other hand, RIN is still the dominant source of noise. In principle, increasing the number of harmonics in the modulation to $N_h = 4$ or more can decrease the RIN. However, we found that even THM produced very little improvement in ARW. The reason for this is still unclear. One possible explanation is that the high frequency of the fifth harmonic ($5\omega/2\pi = 10$ MHz) produces nonlinearity effects in the electronics and optoelectronics that deteriorate the performance of THM. Regarding SHM and DHM, we found good agreement between the theory and experiments.

TABLE II. Estimation of the contribution for each type of noise to the total ARW.

	ARW ($\mu\text{deg}/\sqrt{\text{h}}$)					
	RIN	SN	TPN	DN	Total	Experiment
SHM	8.09	1.41	1.68	0.74	8.42	8.5(2)
DHM	4.67	1.21	1.62	1.03	5.19	5.5(4)
THM	3.56	1.17	1.78	1.10	4.30	5.2(2)

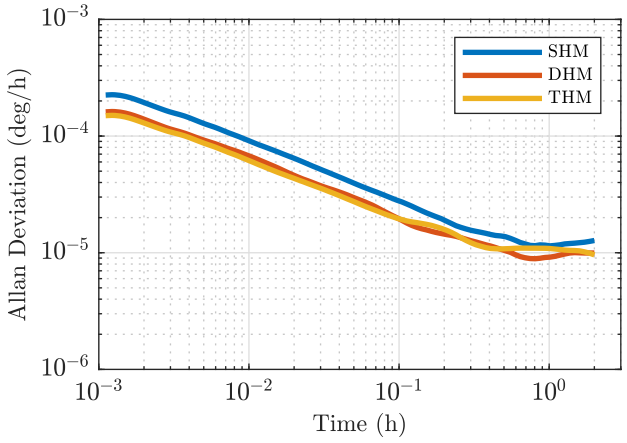

FIG. 5. Allan deviation for 12-hour measurements of SHM, DHM, and THM.

The long-term performance of our FOGs is shown in Fig. 5. The obtained ARWs for SHM, DHM and THM were $9.0(1)\mu\text{deg}/\sqrt{\text{h}}$, $6.5(2)\mu\text{deg}/\sqrt{\text{h}}$, and $6.1(1)\mu\text{deg}/\sqrt{\text{h}}$, respectively. The bias instability was $\sim 10\mu\text{deg/h}$ for the three cases. We observed no degradation of long-time stability due to multiple-harmonic modulation.

VI. CONCLUSION

In this study, we introduced the theory of multi-harmonic modulation, determined optimal parameters for modulation, and experimentally demonstrated improvement of the ARW in an FOG. Regarding the DHM and THM cases, we found that RIN-induced ARW can be reduced by 2.3 dB and 3.7 dB, respectively. We combined the multi-harmonic method with high modulation frequencies to reduce the effects of TPN to obtain an ARW of $5.2\mu\text{deg}/\sqrt{\text{h}}$ and bias instability of $\sim 10\mu$deg/h . This ARW is, to our knowledge, the lowest reported in the world for FOGs. In terms of phase noise, our system reaches a value of 23 nrad/$\sqrt{\text{Hz}}$. This phase noise is 24 times smaller than that obtained with the giant interferometric FOG reported in [13] and 6 times smaller than the phase noise of the iXBlue high-performance prototype FOG reported in [1].

An inertial navigation system (INS) with an accuracy of one nautical mile per month requires a gyro bias below 20 μdeg/h [26]. For initial alignment purposes, reaching this bias precision within one hour requires an angular random walk (ARW) below 20 $\mu\text{deg}/\sqrt{\text{h}}$ [26]. Our system, using either DHM or THM, can reach a minimum bias stability of 10 μdeg/h in less than one hour. With the phase noise reported here, it is possible to reduce the radius of our coil to $R = 30$ mm while maintaining an ARW of $20\mu\text{deg}/\sqrt{\text{h}}$, paving the way for the production of a compact INS with an accuracy of one nautical mile in a month.

To further reduce RIN and TPN, modulation with even higher frequencies and number of harmonics is needed. Ultimately, the bandwidth and linearity of the electronic and optoelectronic components will limit how much RIN and TPN can be decreased using this method. Improving these technologies will be important in the future to increase the precision of FOGs.

ACKNOWLEDGMENT

We thank Y. Kamino for fruitful discussions. We are grateful to H. Ishijima for his technical assistance with the experiments. This work was supported by the Japan Science and Technology Agency (JST) under Grants JPMJPF2015 and JPMJMI17A3.

[1] H. C. Lèfevre, A. Steib, A. Claire, A. Sekeriyan, A. Couderette, A.-L. Pointel, A. Viltard, A. Bonnet, A. Frénois, A. Gandoin, A. Laurent, A. Luton, A. Galbès, A. Ecarnot, B. Cadier, B. Kerouanton, B. Lhermitte, B. Bonnafé, C. Stuber, C. Ortiz, C. Moluçon, C. Allano, C. Dunette, C. Ollivier, C. Guyot, C. Vercambre, D. Ponceau, D. Ramecourt, E. de Toldi, E. Peter, E. Ducloux, E. Vassilakis, F. Colliou, F. Napolitano, F. Lauvinerie, F. Guattari, G. Fauquert, G. Mélin, G. Hardy, G. Lecamp, H. Porte, H. Jaheny, H. Boiron, J.-J. Bonnefois, J.-P. Michel, J.-P. Périot, J. Pillon, J. Hauden, J. Honthaas, K. Aubry, K. Gauthier, L. Lablonde, L. Ly, L. Lhomme, L. Poulain, M. Girault, M. Mancini, M. Goudron, M.-L. Duplaquet, M. Bernasconi, M. Collignon, M. Dacheux, M. Rattier, M. Marta, N. Faussot, N. Grossard, N. Pirrone, O. Jolly, O. Rabine, P. Guitton, P. Mollier, P. Simonpiétri, P. Buisson, P. Cheiney, P. Chakma, R. Taibi, R. Blondeau, S. Shariati, S. Boisgontier, S. Ferrand, S. Keller, S. Huet, S. Chouvin, S. Meyer, S. Puille, S. Ustaze, S. Bénard, S. Clémenceau, T. Laudat, T. Guettler-Sergeant, T. D. Santos, T. Peou-Sanson, T. Robin, T. Buret, T. Loret, T. Villedieu, V. Ferreira, V. D. Pham, V. Rumoroso, Y. Paturel, and H. J. Arditty, "The fiber optic gyro 'adventure' at Photonetics, iXsea and now iXblue," in *Optical Waveguide and Laser Sensors*, R. A. Lieberman, G. A. Sanders, and I. U. Scheel, Eds., vol. 11405, International Society for Optics and Photonics. SPIE, 2020, p. 1140505. [Online]. Available: https://doi.org/10.1117/12.2560791

[2] E. d. Toldi, E. de Toldi, H. Lefèvre, F. Guattari, A. Bigueur, A. Steib, D. Ponceau, C. Molucon, E. Ducloux, J. Wassermann, and U. Schreiber, "First steps for a giant FOG: Searching for the limits," 2017.

[3] C. Schmelzbach, S. Donner, H. Igel, D. Sollberger, T. Taufiqurrahman, F. Bernauer, M. Häusler, C. V. Renterghem, J. Wassermann, and J. Robertsson, "Advances in 6c seismology: Applications of combined translational and rotational motion measurements in global and exploration seismology," *GEOPHYSICS*, vol. 83, no. 3, pp. WC53–WC69, 2018. [Online]. Available: https://doi.org/10.1190/geo2017-0492.1

[4] F. Guattari, C. Moluçon, A. Bigueur, E. Ducloux, E. de Toldi, J. Honthaas, and H. Lefèvre, "Touching the limit of FOG angular random walk: Challenges and applications," in *2016 DGON Intertial Sensors and Systems (ISS)*, Sep. 2016, pp. 1–13.

[5] W. K. Burns and R. P. Moeller, "Noise effects in high sensitivity fiber optic gyros," in *Fiber Optic Gyros: 20th Anniversary Conference*, E. Udd, H. C. Lefevre, and K. Hotate, Eds., vol. 2837, International Society for Optics and Photonics. SPIE, 1996, pp. 381 – 387. [Online]. Available: https://doi.org/10.1117/12.258201

[6] W. K. Burns, R. P. Moeller, and A. Dandridge, "Excess noise in fiber gyroscope sources," *IEEE Photonics Technology Letters*, vol. 2, no. 8, pp. 606–608, 1990.

[7] S. Shin, U. Sharma, H. Tu, W. Jung, and S. A. Boppart, "Characterization and analysis of relative intensity noise in broadband optical sources for optical coherence tomography," *IEEE Photonics Technol. Lett.*, vol. 22, no. 14, pp. 1057–1059, 2010.

[8] J. Blake and I. S. Kim, "Distribution of relative intensity noise in the signal and quadrature channels of a fiber-optic gyroscope," *Opt. Lett.*, vol. 19, no. 20, pp. 1648–1650, Oct 1994. [Online]. Available: http://www.osapublishing.org/ol/abstract.cfm?URI=ol-19-20-1648

[9] A. M. Yurek, H. F. Taylor, L. Goldberg, J. F. Weller, and A. Dandridge, "Quantum noise in superluminescent diodes," *IEEE Journal of Quantum Electronics*, vol. 22, no. 4, pp. 522–527, 1986.

[10] S. Knudsen and K. Bløtekjær, "Interferometric fiber-optic gyroscope performance owing to temperature-induced index fluctuations in the fiber: effect on bias modulation," *Opt. Lett.*, vol. 20, no. 12, pp. 1432–1434, Jun. 1995.

[11] S. Knudsen, A. Tveten, and A. Dandridge, "Measurements of fundamental thermal induced phase fluctuations in the fiber of a sagnac interferometer," *IEEE Photonics Technology Letters*, vol. 7, no. 1, pp. 90–92, 1995.

[12] R. P. Moeller and W. K. Burns, "Observation of thermal noise in a dynamically biased fiber-optic gyro," *Opt. Lett.*, vol. 21, no. 3, pp. 171–173, Feb 1996. [Online]. Available: http://opg.optica.org/ol/abstract.cfm?URI=ol-21-3-171

[13] Y. Li, Y. Cao, D. He, Y. Wu, F. Chen, C. Peng, and Z. Li, "Thermal phase noise in giant interferometric fiber optic gyroscopes," *Opt. Express*, vol. 27, no. 10, pp. 14 121–14 132, May 2019. [Online]. Available: http://www.opticsexpress.org/abstract.cfm?URI=oe-27-10-14121

[14] R. P. Moeller and W. K. Burns, "1.06-μm all-fiber gyroscope with noise subtraction," *Opt. Lett.*, vol. 16, no. 23, pp. 1902–1904, Dec 1991. [Online]. Available: http://ol.osa.org/abstract.cfm?URI=ol-16-23-1902

[15] F. Guattari, S. Chouvin, C. Moluçon, and H. Lefèvre, "A simple optical technique to compensate for excess RIN in a fiber-optic gyroscope," in *2014 DGON Inertial Sensors and Systems (ISS)*, Sep. 2014, pp. 1–14.

[16] P. Polynkin, J. de Arruda, and J. Blake, "All-optical noise-subtraction scheme for a fiber-optic gyroscope," *Opt. Lett.*, vol. 25, no. 3, pp. 147–149, Feb. 2000.

[17] R. C. Rabelo, R. T. de Carvalho, and J. Blake, "SNR enhancement of intensity noise-limited FOGs," *J. Lightwave Technol.*, vol. 18, no. 12, pp. 2146–2150, Dec. 2000.

[18] J. Honthaas, J.-J. Bonnefois, E. Ducloux, and H. Lefèvre, "Interferometric filtering of the excess relative intensity noise of the broadband source of a fiber optic gyroscope," in *23rd International Conference on Optical Fibre Sensors*, J. M. López-Higuera, J. D. C. Jones, M. López-Amo, and J. L. Santos, Eds., vol. 9157, International Society for Optics and Photonics. SPIE, 2014, pp. 329 – 332. [Online]. Available: https://doi.org/10.1117/12.2059578

[19] H. Zhang, X. Chen, X. Shu, and C. Liu, "Fiber optic gyroscope noise reduction with fiber ring resonator," *Appl. Opt.*, vol. 57, no. 25, pp. 7391–7397, Sep 2018. [Online]. Available: https://opg.optica.org/ao/abstract.cfm?URI=ao-57-25-7391

[20] X. Suo, H. Yu, Y. Yang, W. Feng, P. Xie, Y. Chang, Y. He, M. Tang, and Z. Xiang, "Ultralow-noise broadband source for interferometric fiber opticgyroscopesemploying a semiconductor optical amplifier," *Appl. Opt.*, vol. 60, no. 11, pp. 3103–3107, Apr 2021. [Online]. Available: http://opg.optica.org/ao/abstract.cfm?URI=ao-60-11-3103

[21] N. Takei, M. Miranda, Y. Miyazawa, and M. Kozuma, "Simultaneous suppression of thermal phase noise and relative intensity noise in a fiber-optic gyroscope," *IEEE Sensors Journal*, vol. 23, no. 3, pp. 2249–2254, 2023.

[22] T. A. Morris, A. N. Zawada, D. Garcia, J. M. Wheeler, and M. J. F. Digonnet, "Optimization of the angular random walk in Laser-Driven Fiber-Optic gyroscopes," *IEEE Sens. J.*, vol. 22, no. 3, pp. 2205–2212, Feb. 2022.

[23] H. Korsch, A. Klumpp, and D. Witthaut, "On two-dimensional bessel functions," *Journal of Physics A: Mathematical and General*, vol. 39, no. 48, p. 14947, 2006.

[24] P. Kuklinski and D. A. Hague, "Identities and properties of multi-dimensional generalized bessel functions," *arXiv preprint arXiv:1908.11683*, 2019.

[25] P. Combis, P. Cormont, L. Gallais, D. Hebert, L. Robin, and J.-L. Rullier, "Evaluation of the fused silica thermal conductivity by comparing infrared thermometry measurements with two-dimensional simulations," *Applied Physics Letters*, vol. 101, no. 21, p. 211908, 2012. [Online]. Available: https://doi.org/10.1063/1.4764904

[26] Y. Paturel, J. Honthaas, H. Lefèvre, and F. Napolitano, "One nautical mile per month fog-based strapdown inertial navigation system: A dream already within reach?" *Gyroscopy and Navigation*, vol. 5, no. 1, pp. 1–8, Jan 2014. [Online]. Available: https://doi.org/10.1134/S207510871401009X

[27] Y. N. Korkishko, V. A. Fedorov, V. E. Prilutskiy, V. G. Ponomarev, I. V. Fedorov, S. M. Kostritskii, I. V. Morev, D. V. Obuhovich, S. V. Prilutskiy, A. I. Zuev, and V. K. Varnakov, "Highest bias stability fiber-optic gyroscope srs-5000," in *2017 DGON Inertial Sensors and Systems (ISS)*, 2017, pp. 1–23.